

# Ultra-Thin Layered Ternary Single Crystals [Sn(S<sub>x</sub>Se<sub>1-x</sub>)<sub>2</sub>] with Bandgap Engineering for High Performance Phototransistors on Versatile Substrates

Packiyaraj Perumal, Rajesh Kumar Ulaganathan, Raman Sankar, Yu-Ming Liao, Tzu-Min Sun, Ming-Wen Chu, Fang Cheng Chou, Yit-Tsong Chen, Min-Hsiung Shih, and Yang-Fang Chen\*

2D ternary semiconductor single crystals, an emerging class of new materials, have attracted significant interest recently owing to their great potential for academic interest and practical application. In addition to other types of metal dichalcogenides, 2D tin dichalcogenides are also important layered compounds with similar capabilities. Yet, multi-elemental single crystals enable to assist multiple degrees of freedom for dominant physical properties via ratio alteration. This study reports the growth of single crystals Se-doped SnS<sub>2</sub> or SnSSe alloys, and demonstrates their capability for the fabrication of phototransistors with high performance. Based on exfoliation from bulk high quality single crystals, this study establishes the characteristics of few-layered SnSSe in structural, optical, and electrical properties. Moreover, few-layered SnSSe phototransistors are fabricated on both rigid (SiO<sub>2</sub>/Si) and versatile polyethylene terephthalate substrates and their optoelectronic properties are examined. SnSSe as a phototransistor is demonstrated to exhibit a high photoresponsivity of about 6000 A W<sup>-1</sup> with ultra-high photogain ( $\eta$ )  $\approx 8.8 \times 10^5$ , fast response time  $\approx 9$  ms, and specific detectivity ( $D^*$ )  $\approx 8.2 \times 10^{12}$  J. These unique features are much higher than those of recently published phototransistors configured with other few-layered 2D single crystals, making ultrathin SnSSe a highly qualified candidate for next-generation optoelectronic applications.

## 1. Introduction

Since the discovery of graphene and the realization of device fabrication using single layer graphene, atomically thin 2D materials have brought significant excitement and promises for novel device applications.<sup>[1-4]</sup> However, the range of applications for graphene in modern electronics is limited by its gapless nature with no clear on/off states, which is crucial for practical devices such as photodetectors and transistors.<sup>[5-7]</sup> Fortunately, several 2D materials have been discovered to possess a variety of band gap, which enables a new, elementary platform for fashionable in material science, physics, chemistry and engineering. 2D materials have thus raised in advanced device structures and new strategies for device invention that show significant potential in next-generation ultrathin and flexible devices such as phototransistors, optical sensors, light emitting diodes, lasers and high-electron-mobility transistors because

P. Perumal, Y.-M. Liao, T.-M. Sun, Prof. Y.-F. Chen  
Department of Physics  
National Taiwan University  
No. 1, Sec. 4, Roosevelt Road, Taipei 106, Taiwan  
E-mail: yfchen@phys.ntu.edu.tw

P. Perumal, Prof. Y.-F. Chen  
Center for Emerging Material and Advanced Devices  
National Taiwan University  
No. 1, Sec. 4, Roosevelt Road, Taipei 106, Taiwan

P. Perumal, R. K. Ulaganathan  
Nano Science and Technology Program  
Taiwan International Graduate Program  
Academia Sinica and National Taiwan University  
Taiwan

R. K. Ulaganathan, Prof. Y.-T. Chen  
Department of Chemistry  
National Taiwan University  
No. 1, Sec. 4, Roosevelt Road, Taipei 106, Taiwan  
Dr. R. Sankar, Dr. M.-W. Chu, Prof. F. C. Chou  
Center for Condensed Matter Sciences  
National Taiwan University  
No. 1, Sec. 4, Roosevelt Road, Taipei 106, Taiwan  
Dr. M.-H. Shih  
Research Center for Applied Science  
Academia Sinica  
Taipei 115, Taiwan



DOI: 10.1002/adfm.201600081

of their unique dimensional dependent properties.<sup>[8]</sup> Few-layered 2D materials, like graphene, hexagonal boron nitride (h-BN),<sup>[9]</sup> transition metal dichalcogenides (TMDCs),<sup>[10]</sup> such as MoS<sub>2</sub> and WSe<sub>2</sub> and transition metal oxides, are widely established themselves for these significance.<sup>[11–17]</sup> Recent technologies have been dedicated to the invention of latest 2D materials for superior device invention and performance,<sup>[18]</sup> to fulfill the necessities of next-generation technologies and building blocks for novel applications.

In general, 2D exfoliated version of layered materials shows excellent optoelectronic properties as an alternative channel material, distinct from those in graphene. For example, monolayer MoS<sub>2</sub> can exhibit a photoresponsivity as high as  $7.5 \times 10^{-3} \text{ A W}^{-1}$  at a back-gate voltage ( $V_g$ ) 50 V,<sup>[19]</sup> 880  $\text{A W}^{-1}$  at bias voltage ( $V_{ds}$ ) 8 V,<sup>[20]</sup> and the photogain of GaTe can reach 2000%.<sup>[21]</sup> However, almost all 2D materials based phototransistors with higher photogain experience from relatively giant dark currents and low signal/noise ratios (S/N). It will be great beneficial if 2D materials, can possess unique features, such as direct band gap ( $E_g$ ) transition, high crystal quality, valley polarization and Van Hove singularities, which should be able to generate intriguing properties and essential for highly efficient optoelectronic devices.<sup>[22,23]</sup> Moreover, the  $E_g$  of these 2D materials should not be too large in order to sheath a broad spectral range. Recently, few-layered InSe was outlined to possess a band gap of 1.4 eV, creating its feasibility for near-infrared (NIR) phototransistor application.<sup>[8,14]</sup> But for middle IR phototransistors, a fair smaller band gap would be fascinating to enlarge the response even more.

Among all possible 2D materials, thin layers of tin dichalcogenides (SnS<sub>2</sub>, SnSe<sub>2</sub>), member of IV–VI (IV = Sn, Pb, Ge; VI = S, Se, Te) metal dichalcogenides have shown a significant potential for nanoelectronics application due to its great carrier mobility and capability of bandgap engineering, which have driven considerable attention.<sup>[24–29]</sup> Moreover, being earth-abundant, low-cost and environmentally friendly, tin chalcogenides are desirable for sustainable optoelectronic devices. Layered tin dichalcogenides, SnS<sub>2</sub> and SnSe<sub>2</sub>, are both isostructural with the hexagonal cadmium iodide (CdI<sub>2</sub>) type structure and exhibit indirect band gap.<sup>[30,31]</sup> Among this class of layered materials, SnS<sub>2</sub> with a band gap of 2.1 eV, was recently demonstrated a high-performance field-effect transistor (FET) with on/off ratio of  $\approx 10^6$  along with fast photoresponse,<sup>[24,27,30,32]</sup> which is much better than those devices made with GaTe, GaSe, GeSe, MoSe<sub>2</sub>, and so on.<sup>[24,33–36]</sup> The band gap of SnSe<sub>2</sub> is very close to that of silicon (1.1 eV), and was reported to have higher carrier mobility than SnS<sub>2</sub> in bulk form. It is thus of significant interest to find out new 2D layered materials with not only an applicable band gap but also the remarkable optoelectronic properties.<sup>[37]</sup> Selenium doping in SnS<sub>2</sub> thus offers a useful route for bandgap engineering, in that the band gap of Sn(S<sub>x</sub>Se<sub>1-x</sub>)<sub>2</sub> can be continuously fine-tuned from 2.1 eV (SnS<sub>2</sub>) to 1.0 eV (SnSe<sub>2</sub>) by varying selenium content.<sup>[38]</sup> This would provide an important versatility in developing useful devices.

The bulk [Sn(S<sub>0.4</sub>Se<sub>0.6</sub>)<sub>2</sub>] (here after we use as SnSSe) ternary alloy with a band gap around 1.58 eV at room temperature has been used extensively for optoelectronic analysis to assist a new creation of high mobility FETs applications.<sup>[39]</sup> It has isostructural with the hexagonal close packed CdI<sub>2</sub> type

crystal structure similar with that of SnS<sub>2</sub> and SnSe<sub>2</sub>. It exhibits a unique crystal structure (S–Sn–Se strongly bonded covalently) with stacked layers, that act via weak Van Der Waals force between neighboring layers. This allows the creation of well-balanced thin layers with thickness under a few atomic layers, with promise as an important material platform. 2D layered SnSSe thus could probably inherit the outstanding physical properties of bulk SnSSe and even be a good candidate for few-layered 2D material based research. In addition, the consideration of the ultra-thin layered ternary SnSSe alloys can even bring a brand new facet to 2D material analysis. In fact, nowadays, research on 2D materials has been virtually targeted on single and binary elemental systems. Multi-elemental single crystals can lead multiple degrees of freedom for dominant physical properties via ratio variation,<sup>[40]</sup> and in and off itself, few-layered 2D SnSSe ternary compound is a perfect dais for this line of scrutiny.

In this work, we describe the successful synthesis and unambiguously demonstrate the exfoliation of few-layered ( $\approx 6$  nm) SnSSe nanosheets, as an atomically thin 2D layered ternary compound. A thorough study of high performance ultra-thin few-layered ternary SnSSe phototransistors designed on both rigid (SiO<sub>2</sub>/Si) and versatile polyethylene terephthalate (PET) substrates has been performed. The measured carrier mobility of our few-layered SnSSe channel indicates that n-type features of FET, which can reach up to  $\approx 4.6 \text{ V}^{-1} \text{ cm}^2 \text{ s}^{-1}$ . Impressively, the ternary semiconductor of few-layered SnSSe can serve as phototransistors, which is capable of conducting photodetection with preeminent photoresponsivities of up to about  $6000 \text{ A W}^{-1}$  (on SiO<sub>2</sub>/Si) and  $1.2 \text{ A W}^{-1}$  (on PET) at 633 nm, that are predominant to those of reported 2D crystals (SnS<sub>2</sub>, SnSe<sub>2</sub>, MoS<sub>2</sub>, and GaTe) based photodetectors (Table S2 in the Supporting Information). It produces ultra-high gain ( $\eta$ ) over  $\approx 8.8 \times 10^5$  and the measured specific detectivity ( $D^*$ )  $\approx 8.2 \times 10^{12} \text{ J}$  of few-layered SnSSe phototransistor is equivalent to that of commercial silicon (Si) photodiodes. Taking a step further, the photoresponsivities of the SnSSe devices on the versatile PET substrate were explored with and without bending, of that the measured information is inimitable to those on SiO<sub>2</sub>/Si. These figures-of-merit manifest that few-layered SnSSe nanosheets hold a significant potential for device applications, particularly for fabrication of phototransistors with high photoresponse and versatile optoelectronics. The growth of SnSSe single crystals, material characterization, and device fabrication are presented in the experimental section of the Supporting Information.

## 2. Results and Discussion

Figure 1a shows the 3D side view representation of SnSSe crystal structure, which emphasizes the stacking order and Van Der Waals interaction among individual layers within the SnSSe crystal. The distance between each layer is 6.037 Å and also the lattice constant on the *a*-axis is  $\approx 0.34$  nm. The top view of the hexagonal structure of SnSSe crystal is shown in Figure S1 in the Supporting Information. Figure 1b shows the single crystal X-ray diffraction (XRD) pattern of SnSSe crystal. The XRD pattern is identical to the previously reported bulk SnSSe,<sup>[38]</sup> and also the major diffraction peaks are labeled for hexagonal unit

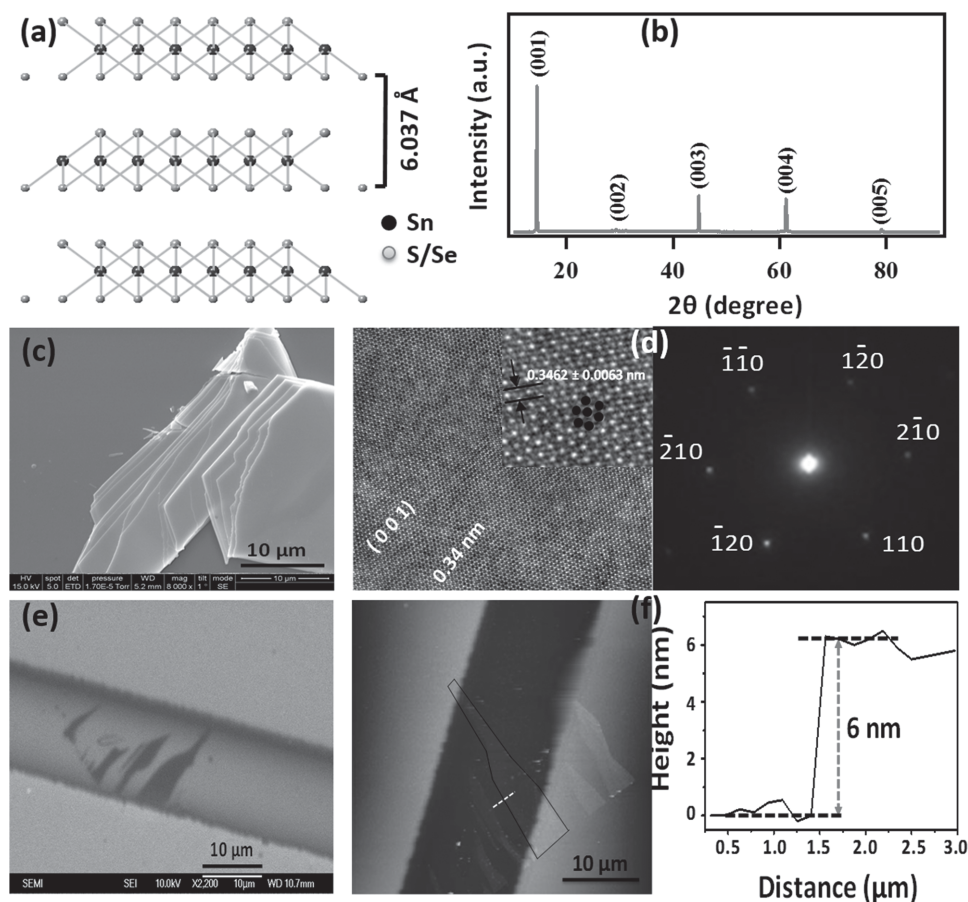


**Figure 1.** Structural characterization of single crystalline and few-layered SnSSe. a) Hexagonal crystal structure of SnSSe (side view model). The layer thickness of SnSSe is 0.6 nm. b) Single crystal XRD pattern of SnSSe. c) FE-SEM image of exfoliated SnSSe nanosheets, which shows a crystal clear layered surface. d) HR-TEM image of few-layered SnSSe nanosheet (inset above shows the lattice constant calculated to be  $\approx 0.34$  nm). SAED pattern (right) of SnSSe nanosheet. e) FE-SEM image of as-fabricated SnSSe phototransistor. f) AFM image of SnSSe phototransistor and height profile (right), shows that smooth surface and 6 nm ( $\approx 10$  atomic layer) thickness.

cells of the CdI<sub>2</sub>-type. SnSSe crystal belongs to the hexagonal Pbnm space group (JCPDS PDF No.23-0677) with lattice constant of  $a = b = 0.364$  nm, and  $c = 0.59$ . The strong diffraction peak at  $\approx 15^\circ$  can be indexed to the (001) plan, while other small periodic diffraction reflections at about  $30.2^\circ$ ,  $46.3^\circ$ ,  $63^\circ$ ,  $78.9^\circ$  are assigned to the (002), (003) (004) (005) planes, respectively. The predominance peak strongly suggests that 2D SnSSe single crystal grows ideally through z-direction with (001) as the bottom plane. The crystal morphology and elemental composition of SnSSe crystal are determined by field-emission scanning electron microscopy (FE-SEM) and energy dispersive X-ray spectroscopy (EDAX). Figure 1c shows FE-SEM image of the SnSSe crystal, which clearly indicates a layered structure. EDX analysis shows the presence of elements, which agrees well with the stoichiometric of SnSSe (Figure S2, Supporting Information). The high resolution transmission electron microscope (HR-TEM) images presented in Figure 1d clearly reveals a naked view of hexagonal structured lattice, which is in good consistency with the atomic model of SnSSe with hexagonal order of Sn, S and Se (inset Figure 1d). The measured lattice fringes from HR-TEM images is about 0.34 nm, that matches very well with  $d$ -spacing (Figure S3, Supporting Information).

The single-crystallinity of the SnSSe nanosheets was investigated by selected area electron diffraction (SAED) oriented along the direction. The diffraction pattern reveals a sixfold symmetry, which confirms the single crystallinity and high quality of SnSSe. In addition, by changing the ratio of S and Se during synthesis, the concentration of Se in the SnS<sub>2</sub> lattice can be well controlled and confirmed by X-ray photoelectron spectroscopy (XPS) analysis. Figure S4 in the Supporting Information exhibits the spectra of binding energies of Sn ( $\approx 486$  eV, and  $\approx 494$  eV), S ( $\approx 161.2$  eV and  $\approx 162.3$  eV), Se ( $\approx 54$  eV), in good agreement with the values from standard values. The electron probe micro-analysis (EPMA) was endorsed to investigate the stoichiometric ratio of the single crystals. Table S1 in the Supporting Information shows that the average elements of Sn, S, and Se are with an atomic ratio of 50%, 20%, and 30%, respectively. Few-layered SnSSe channels were isolated from bulk single crystals by Scotch tape mechanical exfoliation technique and transferred onto SiO<sub>2</sub>/Si with 300 nm thick dielectric layer and then electrically connected to Cr/Au (5/70 nm) electrodes. Figure 1e shows FE-SEM images of exfoliated SnSSe layers on SiO<sub>2</sub>/Si substrate for SnSSe phototransistor. We also performed atomic force microscope (AFM) to probe the surface features

of SnSSe channel. The AFM image of the ultrathin layered SnSSe channel is shown in Figure 1f. The height profile shows in the right corner of Figure 1f, that possess a thickness of  $\approx 6$  nm ( $\approx 10$  atomic layers). Next we use photoluminescence (PL) spectroscopy to examine the optical (excitonic) gap in SnSSe. According to the PL spectrum, the peak position centered at 780 nm for few-layered SnSSe (Figure S5, Supporting Information), corresponding to a band gap of  $1.58 \pm 0.02$  eV. Room temperature ( $T = 300$  K)  $\mu$ PL mappings and corresponding  $\mu$ PL spectra<sup>[32,41]</sup> of representative flakes are shown in Figure S5 in the Supporting Information.

To determine the electronic transport properties of few-layered SnSSe and the potential applications in optoelectronics, we fabricated FET from exfoliated SnSSe flakes. The characteristics of these FET devices were then measured at ambient condition. Figure 2 summarizes the electrical properties of a few-layered back gated SnSSe-FET, which was fabricated using a SnSSe flake ( $\approx 6$  nm thickness). Figure 2a illustrates the schematic representation of the device layout, where degenerately doped Si substrate is used as a back gate and the dielectrics for gate is a 300 nm thick  $\text{SiO}_2$  layer. The top electrodes on SnSSe channel were patterned by thermal evaporator with a breadth of  $\approx 2.9$   $\mu\text{m}$  and also a separation of  $\approx 16.3$   $\mu\text{m}$ . The optical microscope image of  $\approx 6$  nm thin SnSSe phototransistor with two Cr/Au electrodes is shown in Figure 2b. The drain-source current versus drain-source voltage ( $I_{\text{ds}}-V_{\text{ds}}$ ) is measured at different gate voltage ( $V_{\text{g}}$  from  $-40$  V to  $40$  V), which is symmetric and linear over the entire range, indicating ample ohmic contacts.

As shown in Figure 2c, when  $V_{\text{g}}$  is applied,  $I_{\text{ds}}$  increases gradually as the  $V_{\text{g}}$  is changed from  $-40$  V to  $40$  V. Figure 2d plots the source-drain current versus back gate voltage ( $I_{\text{ds}}-V_{\text{g}}$ ) curve measured from  $80$  to  $-80$  V at  $V_{\text{ds}} = 10$  V for the same device. We observe that  $I_{\text{ds}}$  increases with increasing gate voltage, indicating that the electrons, preferably than holes, are the majority carriers within the SnSSe conducting channel. The electron mobility ( $\mu_{\text{e}}$ ) of the few layered SnSSe-FET can be estimated by the following equation  $\mu_{\text{e}} = (L/WCV_{\text{ds}})(dI_{\text{ds}}/dV_{\text{g}})$ , where  $C = \epsilon_0\epsilon_r/d$  (with  $\epsilon_r = 3.9$  and  $d = 300$  nm) is the capacitance for  $\text{SiO}_2$ ,  $W = \approx 2.9$   $\mu\text{m}$  is the channel width, and  $L = \approx 16.3$   $\mu\text{m}$  is the channel length. The calculated  $\mu_{\text{e}}$  of our device is about  $\approx 4.6$   $\text{V}^{-1} \text{cm}^2 \text{s}^{-1}$  and the on/off ratio is  $\approx 10^6$ , which are larger than previously reported few-layered  $\text{SnS}_2$  FETs ( $\approx 1$   $\text{V}^{-1} \text{cm}^2 \text{s}^{-1}$ ).<sup>[32]</sup> The hysteresis behavior for SnSSe phototransistor is shown in Figure S6 in the Supporting Information at a constant drain-source bias ( $V_{\text{ds}} = 10$  V) with different sweeping rates of the  $V_{\text{g}}$ . We can clearly see that the hysteresis behavior is not very pronounced, indicating that the studied device has an excellent quality with a very small amount of trapping centers.

Similar to the back-gate voltage ( $V_{\text{g}}$ ) controlled changes in carrier mobilities, light absorption causes an increase in the carrier mobilities and conductivity of SnSSe channel, allowing them to be used as phototransistors.<sup>[19,20]</sup> Photoconductivity lends itself as a simple approach to photodetection since only the channel resistance needs to be measured and no p-n junction is required to isolate photogenerated electron-hole pairs, investigated at ambient conditions. We calculate the photoresponsivity

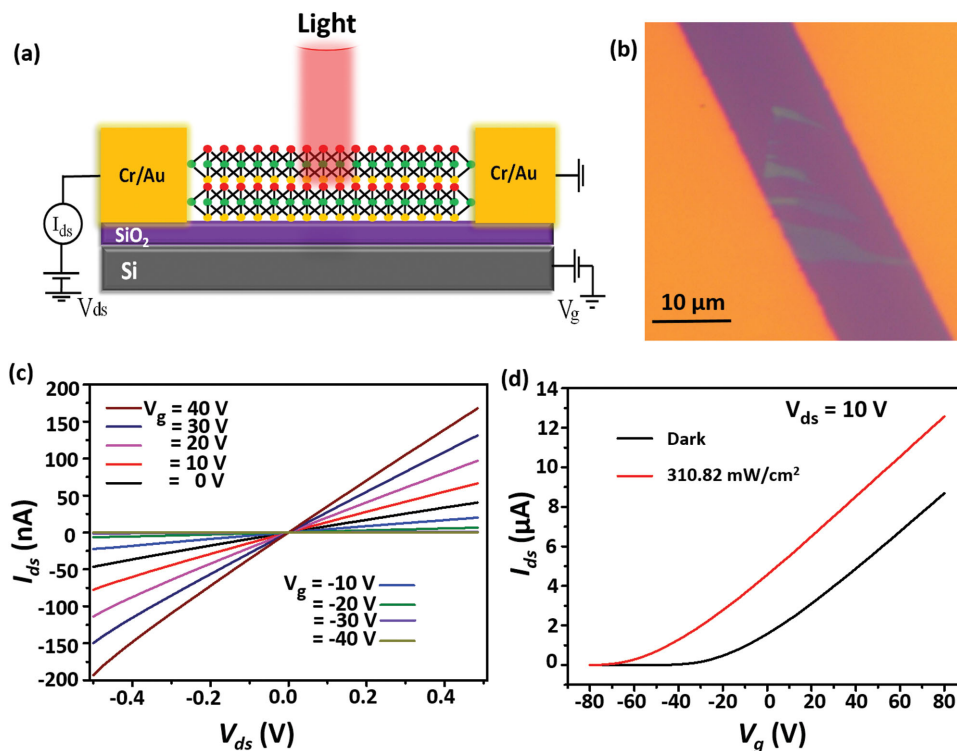


**Figure 2.**  $I$ – $V$  characteristics of few-layered SnSSe phototransistor. a) The schematic illustration represents a few-layered SnSSe phototransistor. b) Optical microscope image of 6 nm thin SnSSe phototransistor separated by 14  $\mu\text{m}$  gap with two Cr/Au electrode. c) The linear  $I_{\text{ds}}-V_{\text{ds}}$  characteristic curve measured at different  $V_{\text{g}}$  from  $-40$  to  $40$  V, represents ohmic behavior. d)  $I_{\text{ds}}-V_{\text{g}}$  characteristic curve measured at  $V_{\text{g}}$  from  $-80$  to  $80$  V at  $V_{\text{ds}} = 10$  V (under dark and laser power of  $310.82$   $\text{mW}/\text{cm}^2$ ).

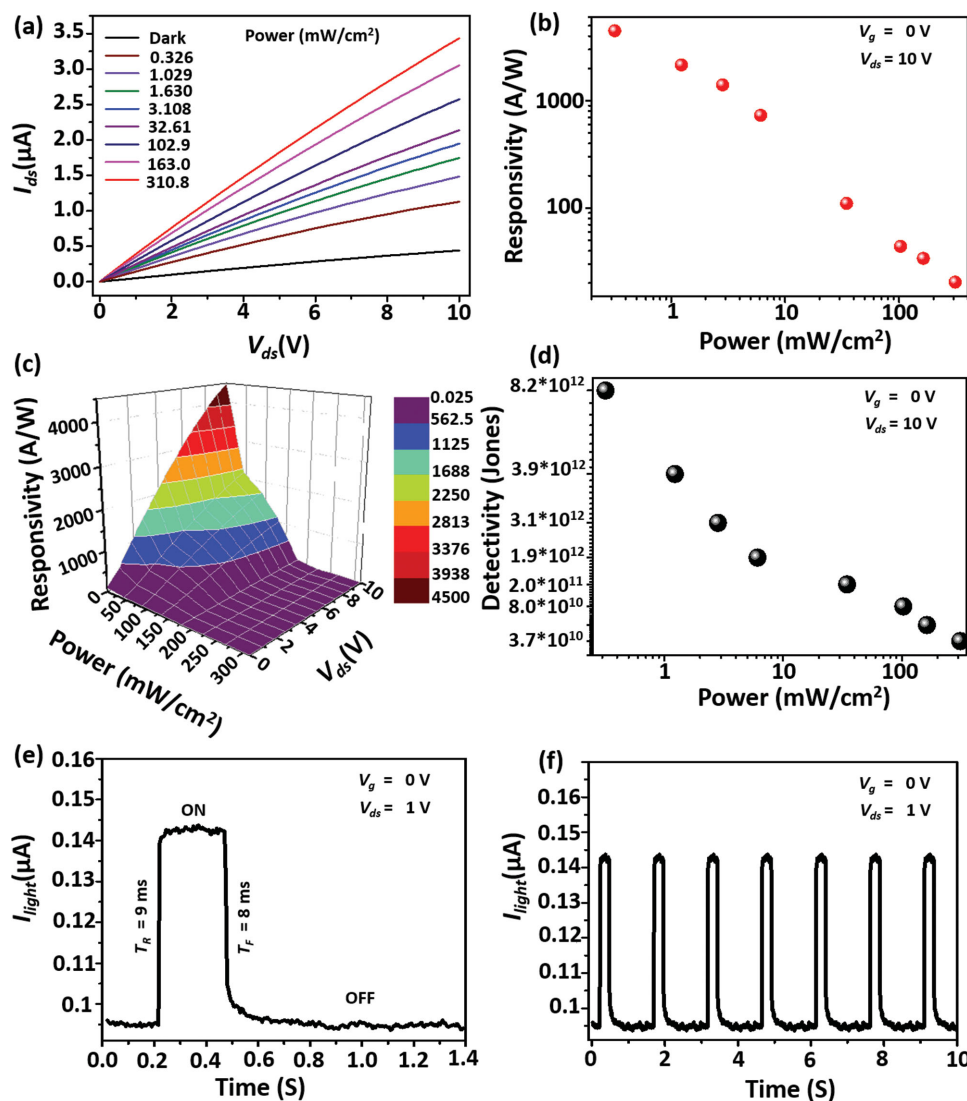


**Figure 3.** Photoresponse study of mechanically exfoliated few-layered (6 nm) SnSSe phototransistor device on a SiO<sub>2</sub>/Si. a) The photoconductivity spectrum of a SnSSe phototransistor acquired at dark and various illuminated power intensities (310.8, 163, 102.9, 32.61, 3.10, 1.63, 1.02, 0.32 mW cm<sup>-2</sup>) without gate bias applied. b) The plot of photoresponsivity versus laser power intensity at V<sub>g</sub> = 0 V and V<sub>ds</sub> = 10 V. c) 3D view of photoresponsivity mapping of few-layered SnSSe phototransistor. d) The plot of detectivity versus laser power intensity at V<sub>g</sub> = 0 V and V<sub>ds</sub> = 10 V. e) The time-resolved photoresponse performance with a time constant of 9 ms and f) photo switching characteristics of the same device measured under 633 nm laser illumination (V<sub>g</sub> = 0 V and V<sub>ds</sub> = 1 V, laser power = 0.326 mWcm<sup>-2</sup>).

of few-layered back-gated SnSSe phototransistor, using a 633 nm laser with different intensities of 310.8, 163, 102.9, 32.61, 3.10, 1.63, 1.02, 0.32 mWcm<sup>-2</sup> and in the dark. **Figure 3a** shows the photoresponsivity spectra of a few-layered (≈6 nm) SnSSe phototransistor with an electrode spacing of 16.3 μm and an effective illumination area of 47 μm<sup>2</sup>. **Figure 3a** exhibits I<sub>ds</sub>–V<sub>ds</sub> plots under the dark and laser illumination, in which the photocurrent (I<sub>ph</sub>) gradually increases as the power gets larger, contrast in the dark. Then, we plot I<sub>ph</sub> versus incident laser power (P) as shown in **Figure S7** in the Supporting Information. The I<sub>ph</sub> arising from photoexcited carrier has a general relation of I<sub>ph</sub> = βP<sup>α</sup>, and in consequence I<sub>ph</sub> increases linearly with power of the laser in both log scale. In SnSSe phototransistor, a similar linear relation was perceived in the low power but the linearity was digressed at high power >30 mWcm<sup>-2</sup> with another

linear slop (**Figure S7**, Supporting Information). At high power illumination, the increase of I<sub>ph</sub> becomes superlinear, which can be attributed to the effects of recombination centers.<sup>[42–44]</sup> When the illumination power of the laser increases, the shift in the quasi Fermi levels makes the lifetime of the carrier longer, turns the recombination rate slower, and leads to the super-linear behavior in the photocurrent observation.

Next we will calculate the responsivity (R<sub>λ</sub>) of the SnSSe phototransistor, which is a significant parameter to conclude the sensitivity of a phototransistor. R<sub>λ</sub>, the I<sub>ph</sub> generated per unit power of illuminated light and area, is extracted as R<sub>λ</sub> = ΔI<sub>λ</sub>/(P<sub>λ</sub>S), where ΔI<sub>λ</sub> is the photocurrent, P<sub>λ</sub> is the power and S is the area of the incident light. **Figure 3b** shows the plot of responsivity versus illumination power. It is clear that the responsivity increases with decreasing illumination power,

which can be contoured effectively with the equation  $R = \alpha E_{\beta}^{-1}$  as shown before.<sup>[24]</sup> The fitting yields the parameter  $\beta = 0.79$ , which is similar to the reported value for few-layered SnS<sub>2</sub> (0.77)<sup>[24]</sup> and few-layered MoS<sub>2</sub> (0.72).<sup>[15]</sup> Remarkably, the maximum  $R_{\lambda}$  of our few-layered SnSSe phototransistor can be up to about 4480 A W<sup>-1</sup> for the 633 nm irradiation at 0.326 mWcm<sup>-2</sup> ( $V_{ds} = 10$  V and  $V_g = 0$  V) and is one order of magnitude above the values recently reported for other 2D crystals based phototransistors (Table S2 in the Supporting Information). Figure 3c exhibits a 3D outlook of the measured  $R_{\lambda}$  (A W<sup>-1</sup>) of a SnSSe phototransistor versus ( $V_{ds} = 0-10$  V,  $V_g = 0$  V) and  $P$  (mWcm<sup>-2</sup>).

Photoresponsivity,  $R_{\lambda} = \Delta I_{\lambda}/(P_{\lambda}S) = [e\alpha/(h\nu)] \cdot (\tau_i/\tau_r)$ , is proportional to the absorption coefficient ( $\alpha$ ) and thickness ( $t$ ) of the channel material at incident photon energy ( $h\nu$ ) and also depends on  $\tau_i/\tau_r$ , which is the ratio of the lifetime of minority carriers ( $\tau_i$ ) to the transit time of majority carriers ( $\tau_r$ ).<sup>[45,46]</sup> Usually, upon light irradiation on the sample, multiple electron-hole pairs are generated. The photoconductivity is enhanced by deferring the recombination of these electron-hole pairs via the trap states to capture the minority carriers to prolong their lifetime ( $\tau_i$ ), meanwhile allowing the majority carriers to have effective, multiple transits across the channel between the source and drain electrodes.<sup>[47-50]</sup> However, this process will induce a very slow response time in the range of seconds, which is not consistent with our measurement. Because the defect states in our studied few-layered Sn(S<sub>x</sub>Se<sub>1-x</sub>)<sub>2</sub> single crystals are very low as demonstrated by the small hysteresis behavior of the  $I-V$  characteristics shown in Figure S6 in the Supporting Information and the pronounced XRD spectra, the above mechanism used to interpret the photoresponse for other 2D materials cannot be the dominant process here. It is believed that the high quality single crystals with low defect density play an important role in our measurement. Due to the low density defects, the minority carrier lifetime increases, which leads to the enhanced photocurrent gain and the fast response time. The high  $R_{\lambda}$  of Sn(S<sub>x</sub>Se<sub>1-x</sub>)<sub>2</sub> phototransistor could also be accounted by the strong absorption<sup>[23,41]</sup> due to the presence of Van Hove singularities in the band structure,<sup>[51,52]</sup> together with the fast, effective separation of photocarriers in the spatial 2D single crystals of Sn(S<sub>x</sub>Se<sub>1-x</sub>)<sub>2</sub> nanosheets to defer electron-hole recombinations arising from the surface band bending caused by large surface area. Note that  $R_{\lambda}$  can be additionally climbed to about 6000 A W<sup>-1</sup> by simply adjusting the gate voltage ( $V_g = 80$  V) as shown in Figure S6 in the Supporting Information. The typical spectral response curve from 400 to 800 nm measured under ( $V_{ds} = 10$  V and  $V_g = 0$  V) and shown in Figure S8 in the Supporting Information.

In general, photoresponsivity not only depends on measurement conditions such as laser power,  $V_g$  and  $V_{ds}$ , but is also strongly related to the device shapes and the barrier at the contact. It is not practical to compare and evaluate directly the responsivity of phototransistor devices fabricated from other 2D layered materials, unless the measurements were done under similar environmental conditions. Therefore, we calculated other two important parameters, specific detectivity ( $D^*$ ) and photogain ( $\eta$ ) of the few-layered SnSSe phototransistors. Photodetectivity is typically calculated with  $D^* = (S \cdot \Delta f)^{1/2}/NEP$ , where  $S$  and  $\Delta f$  are the effective area and electrical bandwidth

of the phototransistor, respectively, and NEP describes noise equivalent power. The NEP is a measure of the least influencing detectable optical power that a phototransistor can differentiate a signal from noise. However, if the phototransistor has a minimum significance of NEP, then the above equation can be modified as  $D^* = R_{\lambda} S^{1/2}/(2eI_{dark})^{1/2}$ , where  $R_{\lambda}$ ,  $S$ ,  $e$ , and  $I_{dark}$  are photoresponsivity, effective area, elementary charge, and dark current, respectively. Recent reports on the calculations of  $D^*$  of 2D materials-based photodetectors have assumed that the shot noise (rather than Johnson noise and thermal fluctuation noise) is the major contribution to the total noise and the detectors exhibiting high photoresponsivity with less dark current have a small NEP.<sup>[24,46,53-55]</sup> In our (SnS<sub>x</sub>Se<sub>1-x</sub>)<sub>2</sub>-FET photodetector, the photoresponsivity ( $R_{\lambda} = 4484$  A W<sup>-1</sup>) is sufficiently high and the dark current (440 nA) is low enough to justify the usage of  $D^* = R_{\lambda} S^{1/2}/(2eI_{dark})^{1/2}$ . The obtained  $D^* \approx 8.2 \times 10^{12}$  J at  $V_g = 0$  for the few-layered SnSSe phototransistor is higher than In<sub>2</sub>Se<sub>3</sub> ( $\approx 2.3 \times 10^{12}$  J)<sup>[53]</sup> and MoS<sub>2</sub> ( $\approx 10^{10}$  to  $\approx 10^{11}$  J)<sup>[56]</sup> phototransistors and equivalent to commercial silicon photodiodes ( $\approx 10^{13}$  J)<sup>[57]</sup> and InGaAs ( $\approx 10^{12}$  to  $\approx 10^{13}$  J).<sup>[58]</sup> Figure 3d reveals the  $D^*$  versus illuminated laser power. Next, we estimate the  $\eta$  of the few-layered SnSSe phototransistor, which is determined by the formula that  $\eta = I_{ph}/e \times E_{ph}/p \times 100\%$ , where  $I_{ph}$  is current difference between dark and illumination,  $e$  is the electron charge,  $E_{ph}$  is the energy of photon, and  $p$  is the illuminated power on the device. The  $\eta$  is the number of electron detected per incident photon and can be expressed as  $\eta = R_{\lambda} hc/e\lambda$ , where  $R_{\lambda}$  is the photoresponsivity,  $h$  is Planck's constant,  $c$  is the speed of light,  $e$  is the elementary charge, and  $\lambda$  is the wavelength of incident light. Here we calculate the  $\eta$  is to be  $\approx 8 \times 10^5$  as shown in Figure S9 in the Supporting Information, which is superior than other 2D based phototransistors as shown Table S2 in the Supporting Information.

Furthermore, the time-resolved evaluations were carried out to exhibit the photoresponse time of the few-layered SnSSe phototransistor. The  $I_{light}-t$  plot was produced with a succession of on/off illumination using 633 nm laser source. Figure 3e presents the device response to a one on/off illumination ( $P = 0.326$  mWcm<sup>-2</sup>,  $V_{ds} = 1$  V, and  $V_g = 0$  V), that exhibits a pointy increase of photocurrent ( $I_{light}$ ) underneath illumination and an instant drop led by a much gentle relaxation after switched off. It is found that the rising time of the device is estimated to be 9 ms, and also the falling time is with a decay of 8 ms. The enlarged scale of rise and decay time was shown in Figure S10 in the Supporting Information. The photoswitching characteristics of time dependent photoresponse were measured for the same device with 633 nm laser on/off ( $V_{ds} = 1$  V, laser power = 0.326 mWcm<sup>-2</sup>) with different cycle is shown in Figure 3f, which indicates the reproducibility of our working device.

In addition, we have performed the responsivity measurements for different Se/S contents as shown in the Figure S11 in the Supporting Information. It indicates that all the responsivities are very high with the device made up of SnS<sub>0.8</sub>Se<sub>1.2</sub> single crystal possessing the highest performance. This behavior can be understood as follows. While increasing the concentration of Se/S ratio, the conduction channel becomes highly electron doped due to higher defect density, which will show a shift in the threshold voltage and the energy separation between the

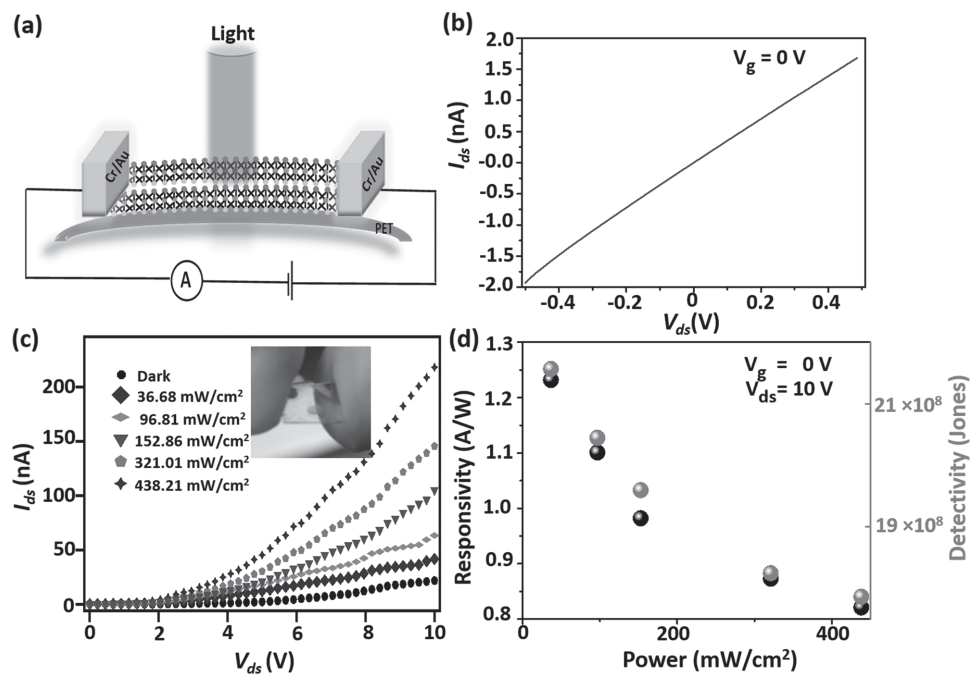


**Figure 4.** Optoelectronic performance of a flexible SnSSe ternary nanosheet phototransistor. a) Schematic diagram illustrates the structure of SnSSe phototransistor on PET. b) The  $I_{ds}$ - $V_{ds}$  characteristics of the few-layered flexible SnSSe phototransistor on PET acquired in the dark. c) Photoconductivity measurements of flexible SnSSe phototransistor on PET, performed at flat state with 633 nm light illumination of 438.21, 321.01, 152.86, 96.81, 36.68  $\text{mW cm}^{-2}$  (inset shows a digital image). d) The plot of photoresponsivity and specific detectivity versus illumination power intensity acquired at flat state ( $V_g = 0$  V and  $V_{ds} = 10$  V).

Fermi level and conduction band minimum is reduced. This reduction will allow more number of excited electrons into the conduction band at room temperature. This observation was clearly demonstrated by Pan et al.<sup>[39]</sup>

Finally, to explore the further applicability of 2D ternary semiconductors, we examined the optoelectronic performance of few-layered SnSSe channel on flexible PET substrate, by the same mechanical exfoliation method. Flexible devices in optoelectronics are another rapidly growing industry with a plenty of promise.<sup>[44,59]</sup> In fact, almost all the 2D materials are stable (except black phosphor) and making themselves the natural alternative for versatile optoelectronics.<sup>[60]</sup> Figure 4a shows the schematic representation of the as-fabricated multi-layered SnSSe device on a PET substrate. The conducting channel of multi-layered SnSSe can stick well onto the surface of PET, exhibiting the device's flexibility. Subsequent thermal deposition of metal electrodes gives rise to mechanically flexible of two terminal electrodes. Analogous to the SnSSe phototransistor made up on  $\text{SiO}_2/\text{Si}$ , this flexible phototransistor additionally holds an ohmic contact, as observed in the  $I_{ds}$ - $V_{ds}$  measurements (Figure 4b). On illumination with 633 nm wavelength of laser, our device becomes conductive due to photoexcited carriers in the SnSSe channel. The illumination power dependent photocurrents recorded in each flat and bent state are shown in Figure 4c and Figure S12a in the Supporting Information, respectively, revealing equivalent performance on the  $\text{SiO}_2/\text{Si}$ . The photocurrent increases with increasing laser power, yielding a highest photoresponsivity of  $1.24 \text{ A W}^{-1}$  at a power density and bias voltage of  $36.68 \text{ mWcm}^{-2}$  and 10 V, respectively, as shown in Figure 4d. Figure 4d plots the responsivity

and specific detectivity versus illumination power. To differentiate the SnSSe phototransistor performance on PET with flat and bending (a radius of  $\approx 2.5$  cm), we observed that the responsivity within the bending state is reduced slightly compared with flat state i.e., the responsivity is slightly reduced to  $0.98 \text{ A W}^{-1}$  under the same measured condition. The reduced responsivity within the bending state is reasonable due to two possible mechanisms. (1) The crack emergence in the electrodes will result in the degeneration of photoexcited carriers. (2) The erected tension in the bending state may additionally reduce the responsivity as a result of the variation of the band structure in the SnSSe channel and its relative optical properties.<sup>[8,44]</sup> In the assessment with an illuminated light intensity of  $36.68 \text{ mWcm}^{-2}$  at 633 nm and  $V_{ds} = 10$  V, the estimated specific detectivities of  $D^* = 22 \times 10^8$  and  $19 \times 10^8 \text{ J}$  for the flat and bending states, respectively, are equivalent. As shown in Figure S13, S14 in the Supporting Information, we demonstrated photoresponse study of the flexible phototransistor on flat and bending state under illumination with a 633 nm at  $15 \text{ mWcm}^{-2}$ , where high reproducibility of photoswitching is observed. These findings reveal a promising potential of the flexible nature of ultra-thin few-layered 2D ternary semiconductors for the excellent practical applications.

### 3. Conclusion

In summary, high-quality single crystalline ternary SnSSe nanosheets were isolated from bulk SnSSe crystal via standard scotch tape exfoliation technique. The phototransistors based

on few-layered (6 nm) ternary SnSSe have been fabricated. The optoelectronic properties of the atomically thin few-layered SnSSe phototransistors with Cr/Au electrodes show an excellent photoresponse under 633 nm illumination. Few-layered SnSSe phototransistors at ambient condition were investigated to provide a very high  $R_{\lambda}$  of  $6000 \text{ A W}^{-1}$  and fast response time of 9 ms (at  $V_g = 0 \text{ V}$ ), which are much better than the recently published values for few-layered 2D single crystals ( $\text{MoS}_2$ , GaTe, and  $\text{SnS}_2$ ) based phototransistors. Moreover, the values of photogain ( $\eta$ )  $\approx 8.8 \times 10^5$  and the measured specific detectivity ( $D^*$ )  $\approx 8.2 \times 10^{12} \text{ J}$  of the few-layered SnSSe phototransistors measured at  $V_g = 0 \text{ V}$  is prominent than those of other 2D single crystals configured phototransistors. We also demonstrated novel flexible phototransistors of few-layered SnSSe fabricated on PET substrate with excellent performance. These properties designate that atomically thin layered ternary SnSSe is an excellent applicant for 2D material based phototransistor applications. Our study shown here provides an excellent illustration that few-layered ternary semiconductors are a highly promising platform for novel optoelectronic device development based on band gap engineering.

## 4. Experimental Section

**Growth of SnSSe Single Crystals:** Single crystalline flakes of  $\text{Sn}(\text{S}_x\text{Se}_{1-x})_2$  were grown by chemical vapor transport (CVT) reaction technique in a horizontal three zone furnace. This study used powders of Sn (99.8%, Alfa Aesar), S (99.5%, Alfa Aesar), Se (99%, Alfa Aesar), and iodine ( $\text{I}_2$ ) in the formation of  $\text{SnI}_4$  as a transport medium. To prepare the pure SnSSe single crystals, the stoichiometric quantity of elements Sn, S:2N, and Se:3N were loaded into high quality conical quartz ampoules evacuated to  $10^{-4} \text{ pa}$  and sealed into the furnace at 873 K for 24 h. Finally, the prereacted 10 g of SnSSe were accommodated with  $\text{SnI}_4$  (5N) at the other end of the ampoule made with silica. The ampoules were heated slowly and maintained 773 K for the time of 1 week. When all was said and done, they were cooled to ambient temperature and the dimensions of the as-grown single crystal were  $8 \times 5 \times 5 \text{ mm}^3$  obtained.

**Mechanical Exfoliation:** As-prepared single crystalline SnSSe flakes were isolated into few-layered SnSSe nanosheets using a mechanical exfoliation (Scotch tap) techniques. Concisely, the bulk SnSSe single crystals were placed on an adhesive tape, and the layers were peeled away by slightly rubbing and slicing. These procedures were repeated several times prior to transferring onto a Si wafer containing a 300 nm thick  $\text{SiO}_2$  dielectric layer, which were examined using an optical microscope (Olympus, BX 51M) equipped with a charge-coupled device (CCD) (Leica, DFC495). The opacity of the SnSSe nanosheets was evaluated from different interference color observed in the optical microscope images and later it was resolved by AFM.

**Device Fabrication:** For the fabrication of device, such as few-layered SnSSe-FETs and phototransistors, SnSSe nanosheets were obtained from the above described method and a TEM copper grid was mounted on exfoliated SnSSe nanosheets on a  $\text{SiO}_2/\text{Si}$  and PET substrate using a homemade micro manipulator. The TEM grid performed as a shadow mask for the deposition of metallic electrodes of Cr/Ar (5 nm/70 nm) by thermal evaporator to fabricate the few-layered SnSSe-FETs.

**Characterization Details:** The lattice constant and hexagonal layered crystal structure were examined with an X-ray diffractometer (Panalytical X'pert PRO) with  $\text{Cu K}\alpha$  radiation ( $\lambda = 1.54056 \text{ \AA}$ ) at ambient temperature in the  $2\theta$  range from  $10$ – $80^\circ$  with a step size of  $0.03939^\circ$ . The layered structure and elements of as-fabricated nanosheets were observed using FE-SEM (JEOL JSM6500), EDAX equipped within the FE-SEM. HR-TEM (Tecnai-G2 F30, accelerating voltage of 300 kv) images were recorded to observe hexagonal lattice structures of as-grown

SnSSe single crystal. XPS (Omicron EA125 analyzer) with Mg  $\text{K}\alpha$  source (1253.6 eV) were used to determine the elemental composition of the as-prepared SnSSe single crystal. AFM (Veeco D3000 NS49) were used to measure the exfoliated nanosheets thickness. The electrical and optical parameters of the device fabricated by few-layered SnSSe were analyzed with the assistance of a probe station (Lakeshore, TTPX) equipped with a source meter (Keithley, 2636A) and an optical system, including a He-Ne laser (JDS Uniphase, Novette 1507), a power meter (Ophit, Nova II), an optical beam shutter (Thorlabs, SH1), a Xenon lamp (Newport, 66921), and a monochromator (Acton, Spectrapro-500). High resolution confocal photoluminescence (PL) microscope (HORIBA, Lab RAM HR) with 488 nm laser was used to take thickness dependent PL image mapping.

## Supporting Information

Supporting Information is available from the Wiley Online Library or from the author.

## Acknowledgements

This work was supported by the National Science Council and Ministry of Education of the Republic of China. The authors P.P and R.K.U thank the support of Taiwan International Graduate Program (TIGP), Institute of Physics, Academia Sinica.

Received: January 6, 2016

Revised: February 15, 2016

Published online: March 15, 2016

- [1] K. S. Novoselov, A. K. Geim, S. V. Morozov, D. Jiang, Y. Zhang, S. V. Dubonos, I. V. Grigorieva, A. A. Firsov, *Science* **2004**, *306*, 666.
- [2] S. Bae, H. Kim, Y. Lee, X. Xu, J. S. Park, Y. Zheng, J. Balakrishnan, T. Lei, H. R. Kim, Y. I. Song, Y. J. Kim, K. S. Kim, B. Ozyilmaz, J. H. Ahn, B. H. Hong, S. Iijima, *Nat. Nanotechnol.* **2010**, *5*, 574.
- [3] T. Mueller, F. Xia, P. Avouris, *Nat. Photonics* **2010**, *4*, 297.
- [4] F. Xia, T. Mueller, Y. M. Lin, A. Valdes-Garcia, P. Avouris, *Nat. Nanotechnol.* **2009**, *4*, 839.
- [5] D. B. Mitzi, L. L. Kosbar, C. E. Murray, M. Copel, A. Afzali, *Nature* **2004**, *428*, 299.
- [6] A. H. Castro Neto, F. Guinea, N. M. R. Peres, K. S. Novoselov, A. K. Geim, *Rev. Mod. Phys.* **2009**, *81*, 109.
- [7] X. Wang, Z. Cheng, K. Xu, H. K. Tsang, J.-B. Xu, *Nat. Photonics* **2013**, *7*, 888.
- [8] S. R. Tamalampudi, Y. Y. Lu, U. R. Kumar, R. Sankar, C. D. Liao, B. K. Moorthy, C. H. Cheng, F. C. Chou, Y. T. Chen, *Nano Lett.* **2014**, *14*, 2800.
- [9] C. R. Dean, A. F. Young, I. Meric, C. Lee, L. Wang, S. Sorgenfrei, K. Watanabe, T. Taniguchi, P. Kim, K. L. Shepard, J. Hone, *Nat. Nanotechnol.* **2010**, *5*, 722.
- [10] L. F. Mattheiss, *Phys. Rev. B* **1973**, *8*, 3719.
- [11] Y. Yoon, K. Ganapathi, S. Salahuddin, *Nano Lett.* **2011**, *11*, 3768.
- [12] S. Lei, L. Ge, Z. Liu, S. Najmaei, G. Shi, G. You, J. Lou, R. Vajtai, P. M. Ajayan, *Nano Lett.* **2013**, *13*, 2777.
- [13] Y. An, A. Behnam, E. Pop, A. Ural, *Appl. Phys. Lett.* **2013**, *102*, 013110.
- [14] S. Lei, L. Ge, S. Najmaei, A. George, R. Kappera, J. Lou, M. Chhowalla, H. Yamaguchi, G. Gupta, R. Vajtai, A. D. Mohite, P. M. Ajayan, *ACS Nano* **2014**, *8*, 1263.
- [15] D. S. Tsai, K. K. Liu, D. H. Lien, M. L. Tsai, C. F. Kang, C. A. Lin, L. J. Li, J. H. He, *ACS Nano* **2013**, *7*, 3905.
- [16] Q. Bao, K. P. Loh, *ACS Nano* **2012**, *6*, 3677.

- [17] P. Hu, Z. Wen, L. Wang, P. Tan, K. Xiao, *ACS Nano* **2012**, *6*, 5988.
- [18] K. Xu, Z. Wang, F. Wang, Y. Huang, F. Wang, L. Yin, C. Jiang, J. He, *Adv. Mater.* **2015**, *27*, 7881.
- [19] Z. Yin, H. Li, H. Li, L. Jiang, Y. Shi, Y. Sun, G. Lu, Q. Zhang, X. Chen, H. Zhang, *ACS Nano* **2011**, *6*, 74.
- [20] O. Lopez-Sanchez, D. Lembke, M. Kayci, A. Radenovic, A. Kis, *Nat. Nanotechnol.* **2013**, *8*, 497.
- [21] Z. Wang, K. Xu, Y. Li, X. Zhan, M. Safdar, Q. Wang, F. Wang, J. He, *ACS Nano* **2014**, *8*, 4859.
- [22] Q. H. Wang, K. Kalantar-Zadeh, A. Kis, J. N. Coleman, M. S. Strano, *Nat. Nanotechnol.* **2012**, *7*, 699.
- [23] L. Britnell, R. M. Ribeiro, A. Eckmann, R. Jalil, B. D. Belle, A. Mishchenko, Y. J. Kim, R. V. Gorbachev, T. Georgiou, S. V. Morozov, A. N. Grigorenko, A. K. Geim, C. Casiraghi, A. H. C. Neto, K. S. Novoselov, *Science* **2013**, *340*, 1311.
- [24] G. Su, V. G. Hadjiev, P. E. Loya, J. Zhang, S. Lei, S. Maharjan, P. Dong, M. A. P. J. Lou, H. Peng, *Nano Lett.* **2015**, *15*, 506.
- [25] H. S. Song, S. L. Li, L. Gao, Y. Xu, K. Ueno, J. Tang, Y. B. Cheng, K. Tsukagoshi, *Nanoscale* **2013**, *5*, 9666.
- [26] Z. Deng, D. Cao, J. He, S. Lin, S. M. Lindsay, Y. Liu, *ACS Nano* **2012**, *6*, 6197.
- [27] D. De, J. Manongdo, S. See, V. Zhang, A. Guloy, H. Peng, *Nanotechnology* **2013**, *24*, 025202.
- [28] Y. Huang, H. X. Deng, K. Xu, Z. X. Wang, Q. S. Wang, F. M. Wang, F. Wang, X. Y. Zhan, J. W. Luo, J. He, *Nanoscale* **2015**, *7*, 14093.
- [29] Y. Huang, K. Xu, Z. X. Wang, T. A. Shifa, Q. S. Wang, F. Wang, C. Jiang, J. He, *Nanoscale* **2015**, *7*, 17375.
- [30] J. Xia, D. Zhu, L. Wang, B. Huang, X. Huang, X.-M. Meng, *Adv. Funct. Mater.* **2015**, *25*, 4255.
- [31] Y. Sun, H. Cheng, S. Gao, Z. Sun, Q. Liu, Q. Liu, F. Lei, T. Yao, J. He, S. Wei, Y. Xie, *Angew. Chem. Int. Ed.* **2012**, *51*, 8727.
- [32] Y. Huang, E. Sutter, J. T. Sadowski, M. Cotlet, O. L. A. Monti, D. A. Racke, M. R. Neupane, D. Wickramaratne, R. K. Lake, B. A. Parkinson, P. Sutter, *ACS Nano* **2014**, *8*, 10743.
- [33] F. Liu, H. Shimotani, H. Shang, T. Kanagasekaran, V. Zolyomi, N. Drummond, V. I. Falko, K. Tanigaki, *ACS Nano* **2014**, *8*, 752.
- [34] M. M. Samani, R. Gresback, M. Tian, K. Wang, A. A. Puretzy, C. M. Rouleau, G. Eres, I. N. Ivanov, K. Xiao, M. A. McGuire, G. Duscher, D. B. Geohegan, *Adv. Funct. Mater.* **2014**, *24*, 6365.
- [35] D. J. Xue, J. Tan, J. S. Hu, W. Hu, Y. G. Guo, L. J. Wan, *Adv. Mater.* **2012**, *24*, 4528.
- [36] J. Xia, X. Huang, L. Z. Liu, M. Wang, L. Wang, B. Huang, D. D. Zhu, J. J. Li, C. Z. Gu, X. M. Meng, *Nanoscale* **2014**, *6*, 8949.
- [37] X. Zhou, L. Gan, W. Tian, Q. Zhang, S. Jin, H. Li, Y. Bando, D. Golberg, T. Zhai, *Adv. Mater.* **2015**, *27*, 8035.
- [38] H. S. Im, Y. Myung, K. Park, C. S. Jung, Y. R. Lim, D. M. Jang, J. Park, *RSC Adv.* **2014**, *4*, 15695.
- [39] T. S. Pan, D. De, J. Manongdo, A. M. Guloy, V. G. Hadjiev, Y. Lin, H. B. Peng, *Appl. Phys. Lett.* **2013**, *103*, 093108.
- [40] S. Lei, A. Sobhani, F. Wen, A. George, Q. Wang, Y. Huang, P. Dong, B. Li, S. Najmaei, J. Bellah, G. Gupta, A. D. Mohite, L. Ge, J. Lou, N. J. Halas, R. Vajtai, P. Ajayan, *Adv. Mater.* **2014**, *26*, 7666.
- [41] P. Yu, X. Yu, W. Lu, H. Lin, L. Sun, K. Du, F. Liu, W. Fu, Q. Zeng, Z. Shen, C. Jin, Q. J. Wang, Z. Liu, *Adv. Funct. Mater.* **2016**, *26*, 137.
- [42] V. Klee, E. Preciado, D. Barroso, A. E. Nguyen, C. Lee, K. J. Erickson, M. Triplett, B. Davis, I. H. Lu, S. Bobek, J. McKinley, J. P. Martinez, J. Mann, A. A. Talin, L. Bartels, F. Leonard, *Nano Lett.* **2015**, *15*, 2612.
- [43] P. Irvin, Y. Ma, D. F. Bogorin, C. Cen, C. W. Bark, C. M. Folkman, C.-B. Eom, J. Levy, *Nat. Photonics* **2010**, *4*, 849.
- [44] D. B. Velusamy, R. H. Kim, S. Cha, J. Huh, R. Khazaeinezhad, S. H. Kassani, G. Song, S. M. Cho, S. H. Cho, I. Hwang, J. Lee, K. Oh, H. Choi, C. Park, *Nat. Commun.* **2015**, *6*, 8063.
- [45] G. W. Mudd, S. A. Svatek, L. Hague, O. Makarovskiy, Z. R. Kudrynskiy, C. J. Mellor, P. H. Beton, L. Eaves, K. S. Novoselov, Z. D. Kovalyuk, E. E. Vdovin, A. J. Marsden, N. R. Wilson, A. Patane, *Adv. Mater.* **2015**, *27*, 3760.
- [46] R. K. Ulaganathan, Y.-Y. Lu, C.-J. Kuo, S. R. Tamalampudi, R. Sankar, K. M. Boopathi, A. Anand, K. Yadav, R. J. Mathew, C.-R. Liu, F.-C. Chou, Y.-T. Chen, *Nanoscale* **2016**, *8*, 2284.
- [47] M. M. Furchi, D. K. Polyushkin, A. Pospischil, T. Mueller, *Nano Lett.* **2014**, *14*, 6165.
- [48] A. R. Klots, A. K. M. Newaz, B. Wang, D. Prasai, H. Krzyzanowska, J. Lin, D. Caudel, N. J. Ghimire, J. Yan, B. L. Ivanov, K. A. Velizhanin, A. Burger, D. G. Mandrus, N. H. Tolc, S. T. Pantelides, K. I. Bolotin, *Sci. Rep.* **2014**, *4*, 6608.
- [49] F. H. L. Koppens, T. Mueller, Ph. Avouris, A. C. Ferrari, M. S. Vitiello, M. Polini, *Nat. Nanotechnol.* **2014**, *9*, 780.
- [50] X. Li, J. E. Carey, J. W. Sickler, M. U. Pralle, C. Palsule, C. J. Vineis, *Opt. Exp.* **2012**, *20*, 5518.
- [51] A. Carvalho, R. M. Ribeiro, A. H. C. Neto, *Phys. Rev. B* **2013**, *88*, 115205.
- [52] R. W. Havener, Y. Liang, L. Brown, L. Yang, J. Park, *Nano Lett.* **2014**, *14*, 3353.
- [53] R. B. J. Gedrim, M. Shanmugam, N. Jain, C. A. Durcan, M. T. Murphy, T. M. Murray, R. J. Matyi, R. L. Moore, B. Yu, *ACS Nano* **2014**, *8*, 514.
- [54] M. Buscema, J. O. Island, D. J. Groenendijk, S. I. Blanter, G. A. Steele, H. S. J. van der Zant, A. C. Gomez, *Chem. Soc. Rev.* **2015**, *44*, 3691.
- [55] P. Hu, L. Wang, M. Yoon, J. Zhang, W. Feng, X. Wang, Z. Wen, J. C. Idrobo, Y. Miyamoto, D. B. Geohegan, K. Xiao, *Nano Lett.* **2013**, *13*, 1649.
- [56] W. Choi, M. Y. Cho, A. Konar, J. H. Lee, G. B. Cha, S. C. Hong, S. Kim, J. Kim, D. Jena, J. Joo, S. Kim, *Adv. Mater.* **2012**, *24*, 5832.
- [57] X. Gong, M. Tong, Y. Xia, W. Cai, J. S. Moon, Y. Cao, G. Yu, C. L. Shieh, B. Nilsson, A. J. Hegger, *Science* **2009**, *325*, 1665.
- [58] J. Kaniewski, J. Piotrowski, *Opto-electron. Rev.* **2004**, *12*, 139.
- [59] Z. Sun, T. Liao, Y. Dou, S. M. Hwang, M. S. Park, L. Jiang, J. H. Kim, S. X. Dou, *Nat. Commun.* **2014**, *5*, 3813.
- [60] M. Chhowalla, H. S. Shin, G. Eda, L. J. Li, K. P. Loh, H. Zhang, *Nat. Chem.* **2013**, *5*, 263.

# ADVANCED FUNCTIONAL MATERIALS

## Supporting Information

for *Adv. Funct. Mater.*, DOI: 10.1002/adfm.201600081

Ultra-Thin Layered Ternary Single Crystals [Sn(S<sub>x</sub>Se<sub>1-x</sub>)<sub>2</sub>] with Bandgap Engineering for High Performance Phototransistors on Versatile Substrates

*Packiyaraj Perumal, Rajesh Kumar Ulaganathan, Raman Sankar, Yu-Ming Liao, Tzu-Min Sun, Ming-Wen Chu, Fang Cheng Chou, Yit-Tsong Chen, Min-Hsiung Shih, and Yang-Fang Chen\**

**Supporting Information**

**Ultra-thin layered ternary single crystals  $[\text{Sn}(\text{S}_x\text{Se}_{1-x})_2]$  with bandgap engineering for high performance photo-transistors on versatile substrates**

*Packiyaraj Perumal, Rajesh Kumar Ulaganathan, Raman Sankar, Yu-Ming Liao, Tzu-Min Sun, Ming-Wen Chu, Fang Cheng Chou, Yit-Tsong Chen, Min-Hsiung Shih, and Yang-Fang Chen\**

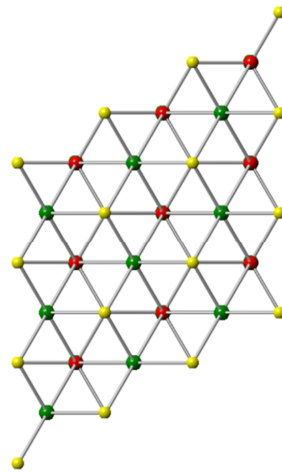


**Figure S1.** Top view of the hexagonal structure of SnSSe crystal.

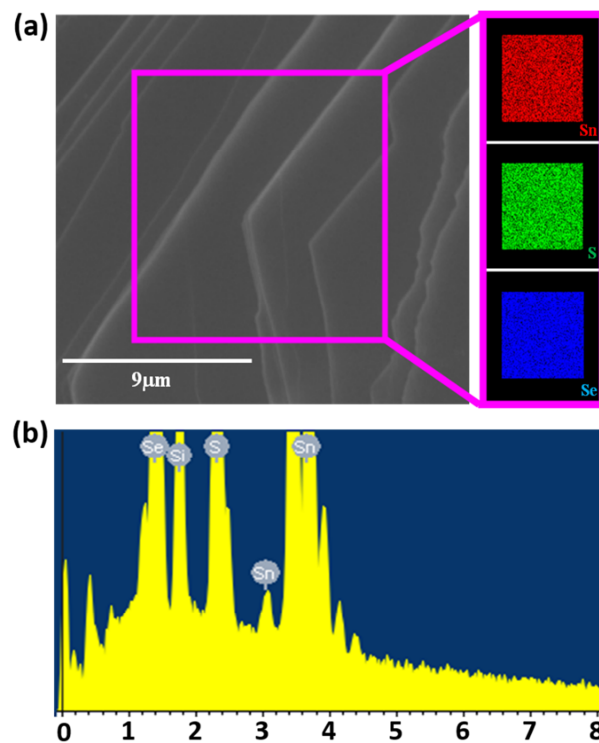


**Figure S2.** (a) FE-SEM image of bulk SnSSe single crystal. The enlarged figures are the elemental mapping for Sn, S and Se, which were produced by energy dispersive X-ray spectroscopy (EDAX) and revealed their homogeneous placements. (b) The EDAX spectrum of SnSSe single crystal.

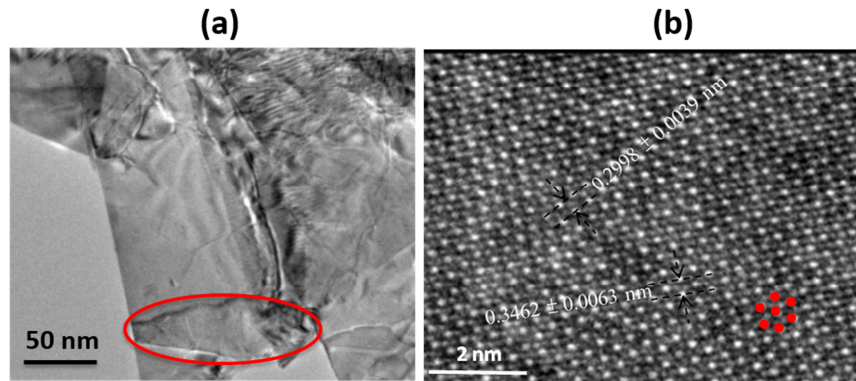


**Figure S3.** (a) High resolution transmission electron microscopy (HR-TEM) images of few-layered SnSSe single crystal. The red circle inside shows that the area focused to capture the images. (b) The image shows the hexagonal lattice structure of SnSSe.

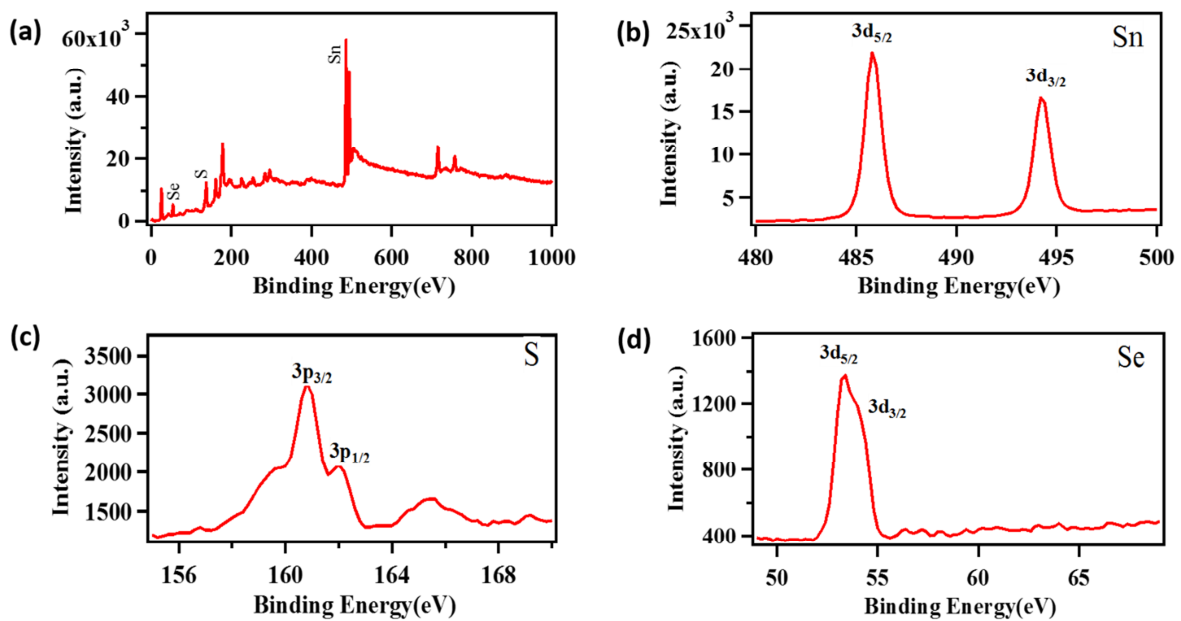


**Figure S4.** X-ray photoelectron spectroscopy (XPS) analysis shows that the spectra of binding energies are corresponds to Sn ( $\sim 486$ , and  $\sim 494$ ) at eV, S ( $\sim 161.2$  and  $\sim 162.3$ ) at eV, Se ( $\sim 54$ ) at eV.

No	Sn	S	Se	Total
1	50.1277	19.2260	30.6463	100.00
2	49.9084	18.9910	31.1006	100.00
3	49.5944	19.4485	30.9571	100.00
4	49.8229	19.4323	30.7448	100.00
5	49.5849	19.6051	30.8100	100.00
<b>Minimum</b>	49.5849	18.9910	30.6463	100.00
<b>Maximum</b>	50.1277	19.6051	31.1006	100.00
<b>Average</b>	49.8076	19.340	30.851	100.00

**Table S1.** The electron probe micro-analysis (EPMA) shows the average elements of Sn, S and Se with an atomic ratio of 50%, 20%, and 30% respectively, signifying a high purity of the synthesized SnSSe single crystal.

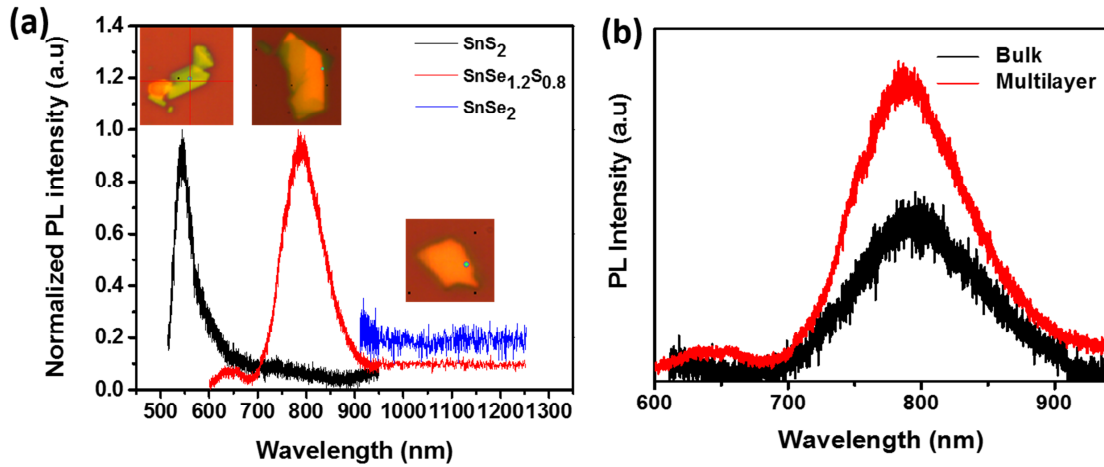


**Figure S5.** Photoluminescence (PL) spectra of bulk and multi-layered  $\text{Sn}(\text{S}_x\text{Se}_{1-x})_2$  at  $T = 300$  K and excitation wavelength of 488 nm laser. (a) PL spectra of multi-layered  $\text{SnS}_2$ ,  $\text{SnSe}_{1.2}\text{S}_{0.8}$  and  $\text{SnSe}_2$ , inset shows the respective  $\mu\text{PL}$  images of the flake on Si wafer. (b)  $\mu\text{PL}$  spectra of bulk and multi-layered  $\text{SnSe}_{1.2}\text{S}_{0.8}$  single crystal.

**Figure S5a** shows the room temperature ( $T = 300\text{K}$ )  $\mu\text{PL}$  mapping and corresponding PL spectra of representative concentration and flakes of  $\text{Sn}(\text{S}_x\text{Se}_{1-x})_2$ . Few-layered  $\text{SnS}_2$  exhibits weak PL at 2.2 eV, indicating the indirect band gap of the nature of the material reported previously<sup>[S1]</sup> We unable to observe any PL emission from bulk to few-layered  $\text{SnSe}_2$  flakes as reported recently.<sup>[S2]</sup> To indicate their stability of the crystals, PL measurements of  $\text{SnSSe}$  flakes persevere for several weeks in the air. Figure S5b shows the PL spectra of bulk and multi-layered flakes of  $\text{SnSe}_{1.2}\text{S}_{0.8}$  single crystal.

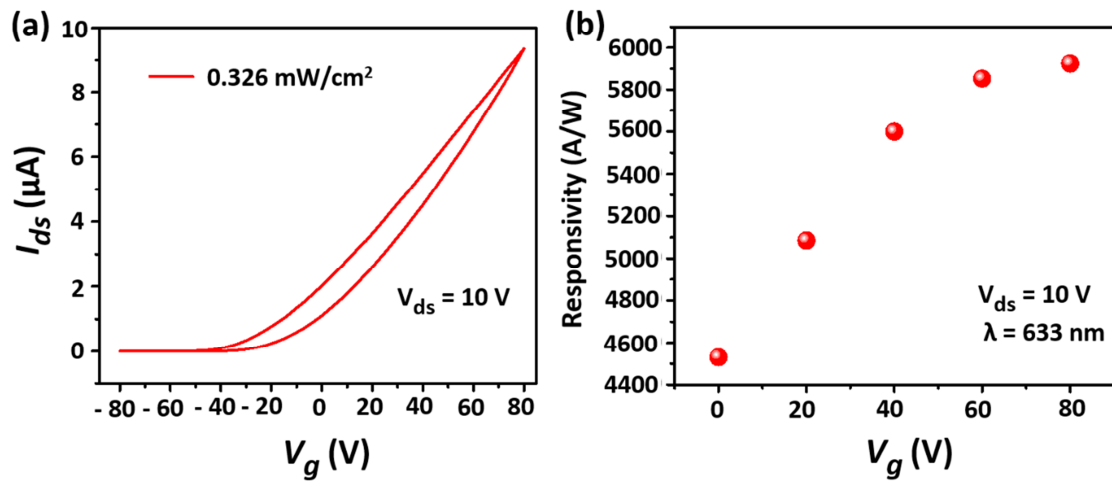


**Figure S6.** (a) Hysteresis behavior of  $I_{ds} - V_g$  (at  $V_{ds} = 10\text{ V}$ ) for broad range of the gate voltage of a few-layered SnSSe photo-transistor. (b) Gate voltage ( $V_g$ ) dependent responsivity of the few-layered SnSSe photo-transistor.

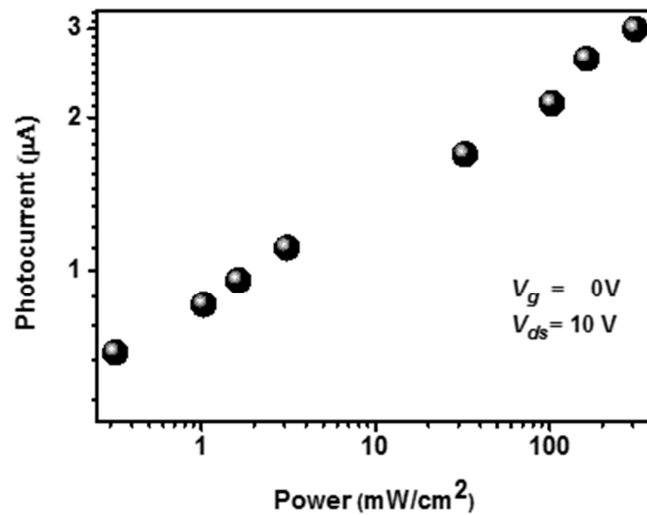


**Figure S7.** The plot of photocurrent versus of laser power intensity at  $V_g = 0\text{ V}$  and  $V_{ds} = 10\text{ V}$ .

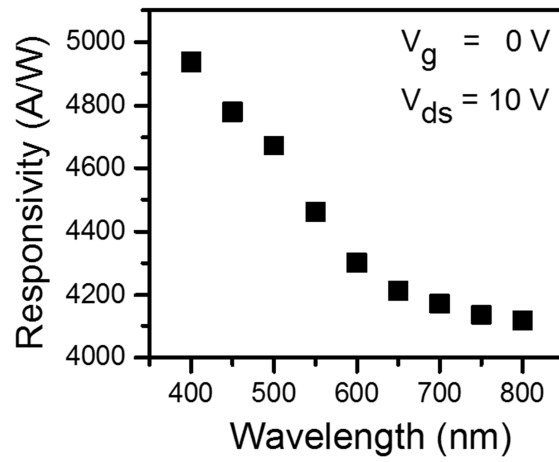


**Figure S8.** The plot of photoresponsivity versus wavelength at  $V_g = 0 \text{ V}$  and  $V_{ds} = 10 \text{ V}$ .

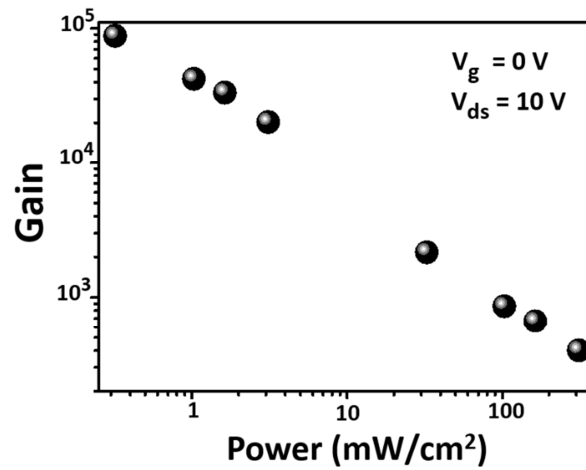


**Figure S9.** The plot of photogain versus laser power intensity at  $V_g = 0 \text{ V}$  and  $V_{ds} = 10 \text{ V}$ .

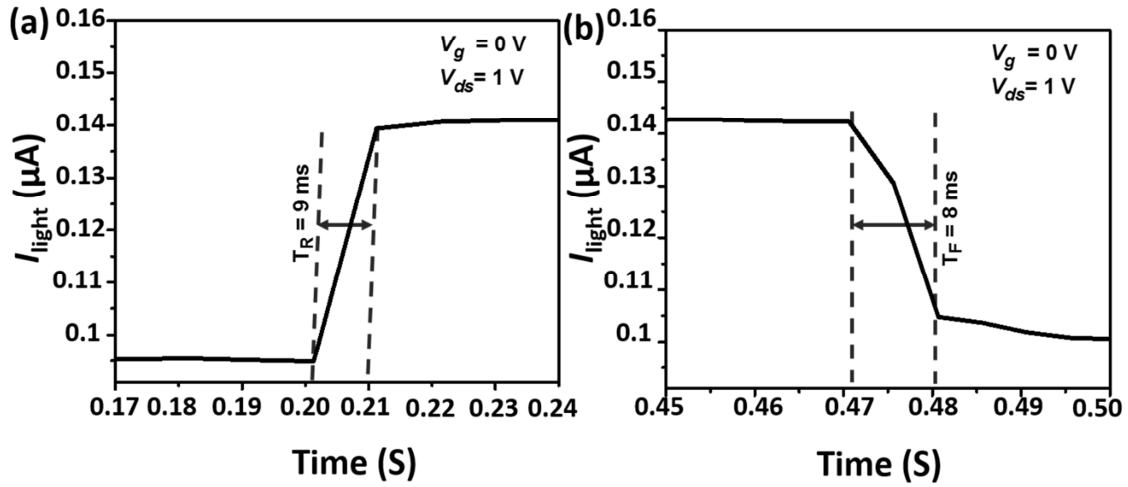


**Figure S10.** The (a) rise and (b) decay time with enlarged scale photoresponse measurement at  $V_g = 0$  V and  $V_{ds} = 1$  V, laser power =  $0.326 \text{ mWcm}^{-2}$ .

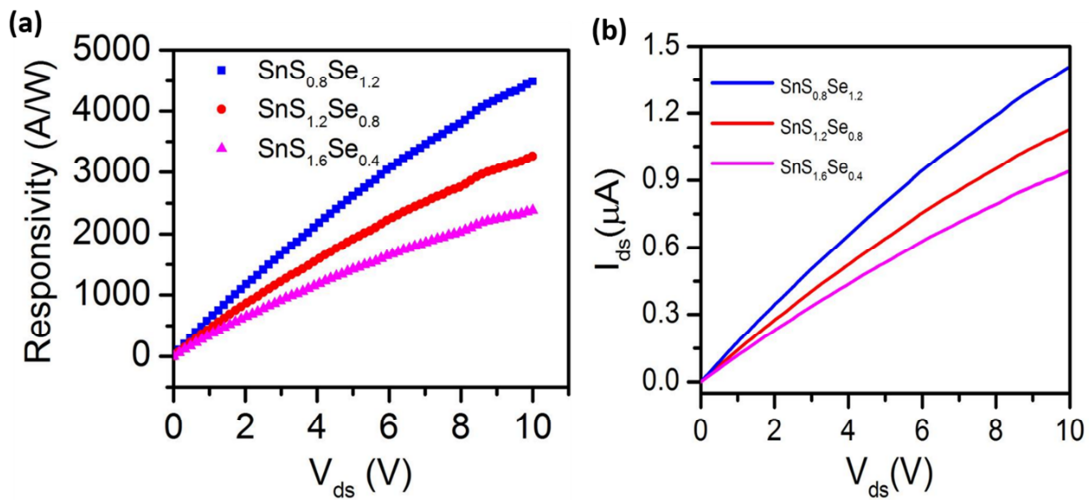


**Figure S11.** (a) Photoresponsivity ( $R_\lambda$ ) of  $\text{Sn}(\text{S}_x\text{Se}_{1-x})_2$  devices under the light illumination of wavelength 633 nm and power density  $P = 0.326 \text{ mWcm}^{-2}$  with a bias voltage of  $V_{ds} = 0\text{-}10$  V and  $V_g = 0$  V. (b) The plot of  $I_{ds}$ - $V_{ds}$  curves for the devices of different ratio of Se/S content in  $\text{Sn}(\text{S}_x\text{Se}_{1-x})_2$  host matrix.

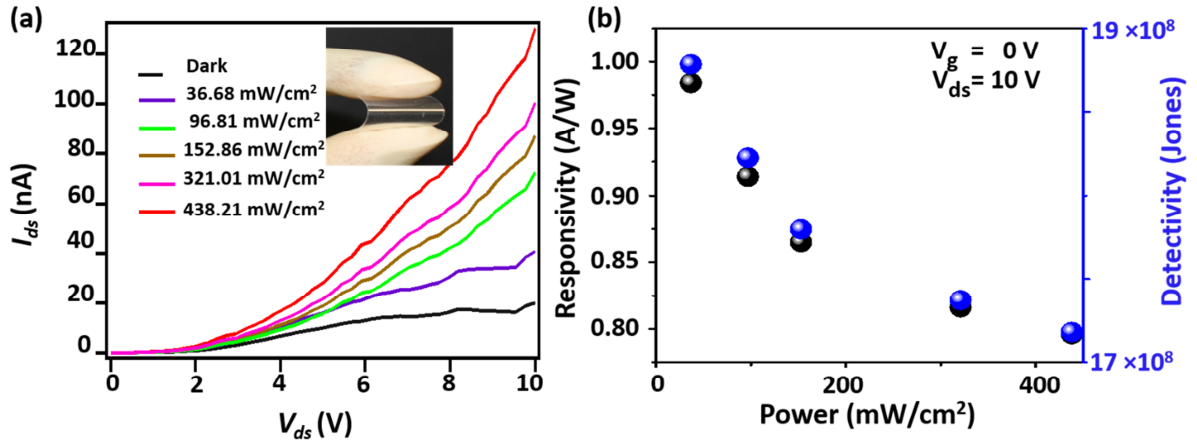


**Figure S12.** Optoelectronic characterization of flexible SnSSe photo-transistor with bending. (a) The  $I_{ds} - V_{ds}$  characteristics of SnSSe photo-transistor fabricated on PET were performed under bending state with 633 nm light illumination of 36.68, 96.81, 152.86, 321.01, 438.21 mWcm<sup>-2</sup> and in the dark. The inset shows a digital image captured with bending state. (b) The plot of responsivity and detectivity versus illumination power intensity calculated in bending states at  $V_g = 0$  V and  $V_{ds} = 10$  V.

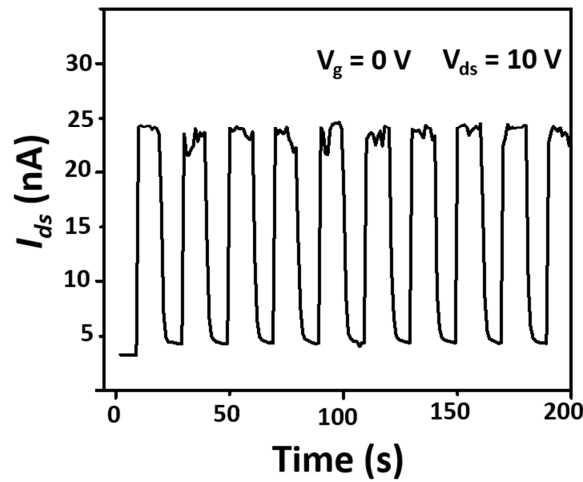


**Figure S13.** The photo-switching measurement for the stability of flexible SnSSe photo-transistor without bending (at  $\lambda = 633$  nm,  $P = 36.68$  mWcm<sup>-2</sup>, and  $V_{ds} = 10$  V).

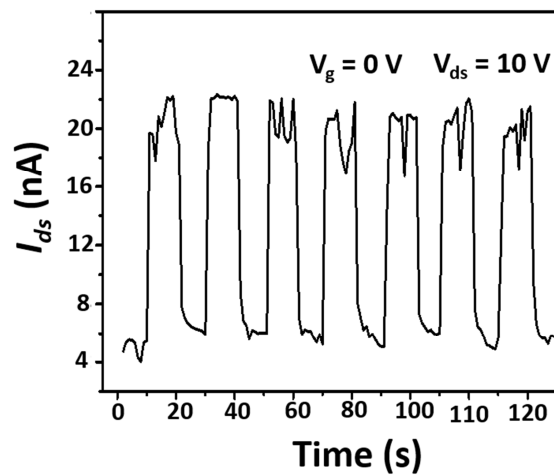


**Figure S14.** The photoswitching measurement for the stability of flexible SnSSe photo-transistor with bending (at  $\lambda = 633\text{ nm}$ ,  $P = 36.68\text{ mWcm}^{-2}$ , and  $V_{ds} = 10\text{ V}$ ).

**Table S2.** Summary of performance metrics of 2D crystal based photo-transistor

Materials	Measurement condition	Responsivity (A/W)	Photogain	Response time	Spectral range	Ref.
Monolayer MoS <sub>2</sub>	561 nm $V_g = -70$ V $V_{ds} = 8$ V	880	NA	4 s	Visible	[S3]
Few-layered In <sub>2</sub> Se <sub>3</sub>	300 nm $V_{ds} = 5$ V	395	$16.3 \times 10^3$	18 ms	UV-Visible	[S4]
Multi-layered GaTe	473 nm $V_{ds} = -5$ V $V_{gs} = -30$ V	800	2000	0.3 s	Visible	[S5]
Multilayered GaTe	532 nm $V_{ds} = 5$ V	100000	NA	6 ms	Visible	[S6]
Ultrathin SnS nanoribbon	532 nm $V_{ds} = 5$ V	NA	$2.3 \times 10^4$	1.1 ms	Visible	[S7]
Multi-layered In <sub>2</sub> Se <sub>3</sub>	300 nm $V_g = 40$ V	98000	$9.8 \times 10^5$	9000 ms	UV-Visible	[S8]
Few-layered CuIn <sub>7</sub> Se <sub>11</sub> (6 nm)	543 nm $V_{ds} = 2$ V	380	88%	24 ms	Visible	[S9]
Few-layered SnS <sub>2</sub>	532 nm $V_{ds} = 20$ V	100	-	44	Visible	[S1]
Few-layered SnSe <sub>2</sub>	530 nm $V_{ds} = 3$ V	1100	$2.6 \times 10^5$	14.5	Visible	[S10]
-----						
Few-layered Present [Sn(Sn <sub>0.6</sub> S <sub>0.4</sub> ) <sub>2</sub> ] on SiO <sub>2</sub> /Si (6 nm)	633 nm $V_g = 0$ V $V_{ds} = 10$ V	4480	$5 \times 10^5$	9 ms	Visible-NIR	work
	$V_g = 80$ V	6000	-	-	„	„
Few-layered Present [Sn(Sn <sub>0.6</sub> S <sub>0.4</sub> ) <sub>2</sub> ] on PET	633 nm $V_g = 0$ V $V_{ds} = 10$ V	1.2 (planar state) 0.9 (bent state)	235 176	-	- Visible-NIR	Visible-NIR work Present work

## References

- [S1] Y. Huang, E. Sutter, J. T. Sadowski, M. Cotlet, O. L. A. Monti, D. A. Racke, M. R. Neupane, D. Wickramaratne, R. K. Lake, B. A. Parkinson, P. Sutter, *ACS Nano* **2014**, *8*, 10743.
- [S2] P. Yu, X. Yu, W. Lu, H. Lin, L. Sun, K. Du, F. Liu, W. Fu, Q. Zeng, Z. Shen, C. Jin, Q. J. Wang, Z. Liu, *Adv. Funct. Mater.* **2016**, *26*, 137.
- [S3] Z. Yin, H. Li, H. Li, L. Jiang, Y. Shi, Y. Sun, G. Lu, Q. Zhang, X. Chen, H. Zhang, *ACS Nano* **2012**, *6*, 74.
- [S4] R. B. J. Gedrim, M. Shanmugam, N. Jain, C. A. Durcan, M. T. Murphy, T. M. Murray, R. J. Matyi, R. L. Moorell, B. Yu, *ACS Nano* **2014**, *8*, 514.
- [S5] Z. Wang, K. Xu, Y. Li, X. Zhan, M. Safdar, Q. Wang, F. Wang, J. He, *ACS Nano* **2014**, *8*, 4859.
- [S6] F. Liu, H. Shimotani, H. Shang, T. Kanagasekaran, V. Zolyomi, N. Drummond, V. I. Falko, K. Tanigaki, *ACS Nano* **2014**, *8*, 752.
- [S7] Z. Deng, D. Cao, J. He, S. Lin, S. M. Lindsay, Y. Liu, *ACS Nano* **2012**, *6*, 6197.
- [S8] J. O. Island, S. I. Blanter, M. Buscema, H. S. J. van der Zant, A. C. Gomez, *Nano Lett.* **2015**, *15*, 7853.
- [S9] S. Lei, A. Sobhani, F. Wen, A. George, Q. Wang, Y. Huang, P. Dong, B. Li, S. Najmaei, J. Bellah, G. Gupta, A. D. Mohite, L. Ge, J. Lou, N. J. Halas, R. Vajtai, P. Ajayan, *Adv. Mater.* **2014**, *26*, 7666.
- [S10] X. Zhou, L. Gan, W. Tian, Q. Zhang, S. Jin, H. Li, Y. Bando, D. Golberg, T. Zhai, *Adv. Mater.* **2015**, *27*, 8035.